Analysis of the Characteristics of an Earthed Fin Line

ADALBERT BEYER

Abstract—**This paper presents a theoretical and experimental investigation of the effective permittivity and the characteristic impedance of the earthed unilateral fin line. Using the Ritz–Galerkin method, the eigenvalue equation for a fin line with finite metallization thickness as well as a longitudinal slit in the metal waveguide mount is derived.**

The numerical solution converges very rapidly in all the cases investigated.

Experimental checks are reported, which verify the results of this method and stress the importance of the effects of the finite metallization thickness and longitudinal slit in the mount at higher frequencies.

The theoretical results are compared with results by Hofmann, and they are found to correspond closely.

I. Introduction

IN NEWLY DEVELOPED millimeter-wave circuits planar lines are used to integrate components and subsystems. Besides microstrip lines, suspended substrate lines and coplanar lines, especially fin lines, are employed, which lead to a high flexibility in the realization of the circuits.

In earthed fin lines metal fins are printed on a dielectric substrate, which bridge the walls of a rectangular waveguide (Fig. 1).

Up to now, several papers have been published describing experimental and theoretical investigations of fin lines [2], [3], [7], [8]. The agreement of measured and calculated propagation constants generally is unsatisfactory. This especially is true for high millimeter-wave frequencies. The discrepancies result from neglecting the effects of the finite metallization thickness of the fins and from neglecting the effects of the slits in the fin-line mounts (Fig. 1).

Only for very thin metallization layers (e.g., evaporated gold or copper layers with 1–5-μm thickness) the assumption of vanishing metallization thickness is justified as an approximation. In practical cases, however, where commercially available copper-clad substrate materials are used with copper thicknesses ranging between 20 and 100 μm, errors of 5 to 8 percent (E-band values) in the effective dielectric constant ϵ_{eff} of the fin lines are due the disregarding the effects of the finite metallization thickness. This is especially true in the case of low-impedance fin lines needed in semiconductor circuits, where the slot width $2s$ is very small compared to the narrow wall dimension b of the waveguide mount (Fig. 2).

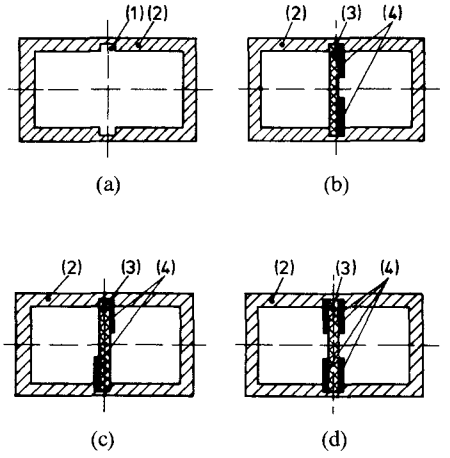

Fig. 1 Cross sections of earthed fin lines: (a) waveguide mount, (b) unilateral fin line, (c) antipodal fin line, (d) bilateral fin line. 1) Slit, 2) metal wall, 3) dielectric substrate, 4) metal fin.

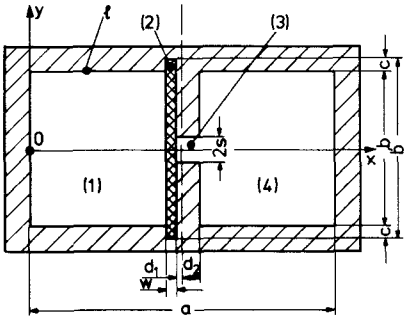

Fig. 2. Cross section of the unilateral earthed fin line for E=band. $a=3.099\pm0.02$ mm, $b=1.549\pm0.02$ mm, $b'=2.2$ mm, $d_1=0.01$ mm, $d_2=0.06$ mm, $w=0.05$ mm, $c=0.326$ mm, 0.05 mm$\leqslant s\leqslant$0.5 mm.

The effects due to the slit in the waveguide mount Fig. 1(a) especially are important for small fin lines in the higher millimeter-wave frequency range, e.g., at E-band, although the connected errors can be reduced by reducing the slit height c (Fig. 2). Errors of 3 to 5 percent can occur in the effective dielectric constant ϵ_{eff} and the characteristic impedance Z_0 due to neglecting the effects of the slit in the waveguide mount. However, unlike the errors due to the finite metallization thickness, these errors are most critical for high-impedance fin lines which are important in filters and transitions, where the slot width is large ($2s \cong b$).

Manuscript received May 13, 1980; revised January 26, 1981. A condensed version of this paper has been presented at the 1980 IEEE-MTTS International Microwave Symposium, Washington, DC.

The author is with the Department of Electrical Engineering, University of Duisburg, D-4100 Duisburg 1, Federal Republic of Germany.

0018-9480/81/0700-0676$00.75 ©1981 IEEE

II. The Eigenvalue Problem of the Unilateral Fin Line

In the following, a calculation method for all known fin-line configurations (Fig. 1(b), (c), (d)) is described which takes into account both the finite metallization thickness and the finite longitudinal slit in the waveguide mount. In view of the fact that the bilateral fin line has been treated in several papers [3], [8] while the unilateral fin line has been treated more scarcely, the method presented in this paper is applied to the unilateral fin line.

The present treatment is based on the ridge-loaded waveguide model for unilateral earthed fin lines [5], [6] and takes into account the finite thickness of the metal fin, the longitudinal slit of the waveguide mount, and the cross-sectional symmetry with respect to the x-axis.

Let Fig. 2 represent the cross section of an unilateral fin line with conducting boundary l. The electromagnetic field in each subregion 1), 2), 3), or 4) can be described using scalar functions Φ and Ψ.

With respect to the boundary conditions on the metallic walls, the scalar potentials are written in subregion 1) as

$$\Phi^{(1)} = \sum_{m=1}^{\infty} A_m \sin\left(\bar{k}_{xm}^{(1)} x\right) \sin\left[\bar{k}_{ym}^{(1)}(y-b/2)\right], \qquad 0<x<a/2-(w+d_1)$$

$$\Psi^{(1)} = \sum_{n=0}^{\infty} B_n \cos\left(k_{xn}^{(1)} x\right) \cos\left[k_{yn}^{(1)}(y-b/2)\right], \qquad 0<x<a/2-(w+d_1) \quad (1)$$

where

$$\bar{k}_{ym}^{(1)} = \frac{m\pi}{b} \qquad k_{yn}^{(1)} = \frac{n\pi}{b}. \quad (2)$$

In subregion 2) the potentials are written as

$$\Phi^{(2)} = \sum_{m=1}^{\infty} \left[C_m \cos\left(\bar{k}_{xm}^{(2)} x\right) + D_m \sin\left(k_{xm}^{(2)} x\right)\right] \cdot \sin\left[\bar{k}_{ym}^{(2)}(y-b'/2)\right], \qquad a/2-(w+d_1)<x<a/2-d_1$$

$$\Psi^{(2)} = \sum_{n=0}^{\infty} \left[F_n \cos\left(k_{xn}^{(2)} x\right) + G_n \sin\left(k_{xn}^{(2)} x\right)\right] \cdot \cos\left[k_{yn}^{(2)}(y-b'/2)\right], \qquad a/2-(w+d_1)<x<a/2-d_1 \quad (3)$$

where $\bar{k}_{ym}^{(2)}$ and $k_{yn}^{(2)}$ are defined analogously to $\bar{k}_{ym}^{(1)}$ and $k_{yn}^{(1)}$, respectively.

The scalar potentials in subregion 3) are given by

$$\Phi^{(3)} = \sum_{m=1}^{\infty} \left[H_m \cos\left(\bar{k}_{xm}^{(3)} x\right) + K_m \sin\left(\bar{k}_{xm}^{(3)} x\right)\right] \cdot \sin\left[\bar{k}_{ym}^{(3)}(y-s)\right], \qquad a/2-d_1<x<a/2+d_2$$

$$\Psi^{(3)} = \sum_{n=0}^{\infty} \left[L_n \cos\left(k_{xn}^{(3)} x\right) + N_n \sin\left(k_{xn}^{(3)} x\right)\right] \cdot \cos\left[k_{yn}^{(3)}(y-s)\right], \qquad a/2-d_1<x<a/2+d_2 \quad (4)$$

where

$$\bar{k}_{ym}^{(3)} = \frac{m\pi}{2s} \qquad k_{yn}^{(3)} = \frac{n\pi}{2s}. \quad (5)$$

Finally, in subregion 4) it is appropriate to write

$$\Phi^{(4)} = \sum_{m=1}^{\infty} P_m \sin\left[\bar{k}_{xm}^{(4)}(x-a)\right] \sin\left[\bar{k}_{ym}^{(4)}(y-b/2)\right], \qquad a/2+d_2<x<a$$

$$\Psi^{(4)} = \sum_{n=0}^{\infty} R_n \cos\left[k_{xn}^{(4)}(x-a)\right] \cos\left[k_{yn}^{(4)}(y-b/2)\right], \qquad a/2+d_2<x<a \quad (6)$$

where $\bar{k}_{ym}^{(4)}$ and $k_{yn}^{(4)}$ can be given by analogy with (2). The separation parameter equations in the four subregions are

$$\bar{k}_{xn}^{(i)2} + \bar{k}_{yn}^{(i)2} + \beta_n^2 = k_{xn}^{(i)2} + k_{yn}^{(i)2} + \beta_n^2 = \epsilon_r^{(i)} k_0^2, \qquad i=1,2,3,4 \quad (7)$$

where

$$k_0^2 = \omega^2 \epsilon_0 \mu_0. \quad (8)$$

It can be shown that the electromagnetic fields of subregion 2) can be matched to the electromagnetic fields of subregion 3) over their common interface, in the example mentioned, at $x=a/2-d_1$.

As an example, the calculation method is demonstrated for the odd TE modes [6]. Applying the continuity of the odd TE-mode field Ψ at the interface $x=a/2-d_1$, we get the following equation:

$$\sum_{n=0}^{\infty} G_n \sin\left\{k_{xn}^{(2)}\left(\frac{a}{2}-d_1\right)\right\} \cos\left\{k_{yn}^{(2)}\left(y-\frac{b'}{2}\right)\right\} = \sum_{m=0}^{\infty} N_m \sin\left\{k_{xm}^{(3)}\left(\frac{a}{2}-d_1\right)\right\} \cos\left\{k_{ym}^{(3)}(y-s)\right\}. \quad (9)$$

The $E_y^{(2)}$ and $E_y^{(3)}$ fields at both sides of the interface $x=a/2-d_1$ may be represented by an integral expression [6] which yields the coefficients G_n and N_m

$$G_n = \frac{\nu_n \cdot \int_{b'/2}^{b'/2} E_y^{(2)}\left(\frac{a}{2}-d_1, y\right) \cos\left\{k_{yn}^{(2)}\left(y-\frac{b'}{2}\right)\right\} dy}{j\omega\mu k_{xn}^{(2)} b' \cos\left\{k_{xn}^{(2)}\left(\frac{a}{2}-d_1\right)\right\}} \quad (10)$$

$$N_m = \frac{\nu_m \cdot \int_{-s}^{s} E_y^{(3)}\left(\frac{a}{2}-d_1, y\right) \cos\left\{k_{ym}^{(3)}(y-s)\right\} dy}{j\omega\mu k_{xm}^{(3)} 2s \cos\left\{k_{xm}^{(3)}\left(\frac{a}{2}-d_1\right)\right\}} \quad (11)$$

where $\nu_n = \nu_m = 1$ for $n=m=0$ and $\nu = \nu_m = 2$ for $n>0$ and $m>0$ (Neumann's numbers). Substitutions of (10) and (11)

into (9) gives

$$\sum_{n=0}^{\infty} \frac{\nu_n \cdot \tan\left\{k_{xn}^{(2)}\left(\frac{a}{2}-d_1\right)\right\} \cdot \cos\left\{k_{yn}^{(2)}\left(y-\frac{b'}{2}\right)\right\}}{k_{xn}^{(2)} b'}$$

$$\times \int_{-b'/2}^{b'/2} E_y^{(2)}\left(\frac{a}{2}-d_1, y\right) \cos\left\{k_{yn}^{(2)}\left(y-\frac{b'}{2}\right)\right\} dy$$

$$= \sum_{m=0}^{\infty} \frac{\nu_m \cdot \tan\left\{k_{xm}^{(3)}\left(\frac{a}{2}-d_1\right)\right\} \cdot \cos\left\{k_{ym}^{(3)}(y-s)\right\}}{2k_{xm}^{(3)} s}$$

$$\times \int_{-s}^{s} E_y^{(3)}\left(\frac{a}{2}-d_1, y\right) \cos\left\{k_{ym}^{(3)}(y-s)\right\} dy. \quad (12)$$

The characteristic equation arrived at now has the form of

$$\sum_{n=0}^{\infty} T_{mn}(k_n) \cdot S_n = 0, \qquad m=0,1,2,\cdots \quad (13)$$

where S_n is the amplitude vector. For practical calculations, the number of equations as well as the number of modes considered cannot be increased indefinitely. Therefore, the number of equations in (13) is limited to $m_{\max}$ and the number of amplitudes is limited to $n_{\max}$. Thus the characteristic equation is reduced to a finite system of homogeneous equations. It is sufficient to choose $m_{\max}=n_{\max}$ to search for solutions for the $n_{\max}$ modes considered in the calculations.

The characteristic equation

$$\sum_{n=0}^{n=n_{\max}} T_{mn}(k_n) \cdot S_n = 0, \qquad m=0,1,2,\cdots,n_{\max} \quad (14)$$

possesses a nontrivial solution, if its determinant vanishes

$$\det\{T_{mn}(k_{cn})\} = 0 \quad (15)$$

which also is the formulation for the eigenvalue problem. With the wavenumbers k_{cn} known from the zeros of the eigenvalue equation (15), the corresponding modes S_n can be calculated from (14) except for a constant factor.

Equations (9)–(12) were applied to the geometry shown in Fig. 2 (E-band fin lines). The method, in general, converges very rapidly: In all the cases investigated, a minimum number of only 10 modes in the slot (subregion 3)) and in the substrate (subregion 2)) is needed for a sufficient accuracy of the calculated eigenvalues. The typical execution time for one frequency point on a Cyber 76 computer is about 4 s.

III. Theoretical and Experimental Results

The experimental verification of the theoretical results was restricted to the fundamental mode on the fin line. Measurements were made using a precision slot line for the measurement of the input VSWR of the fin line and a movable short in the fin-line section. The fin lines employed in the experiments were 24.2 mm long, which corresponds to more than three wavelengths at the lowest measuring frequency. The fin-line substrate used in the experiments was Kapton foil ($\epsilon_r=3.0, w=0.05$ mm) clad with plated gold ($d=10$ μm) and rolled copper ($d=70$ μm).

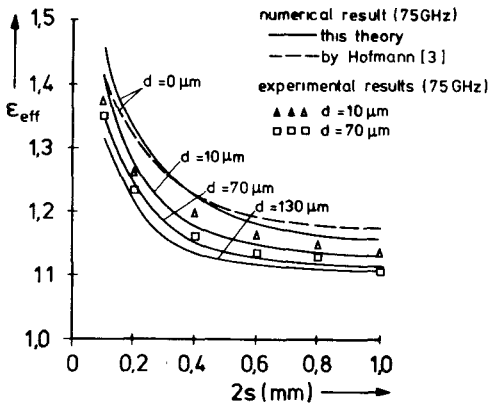

Fig. 3. Equivalent dielectric constant (ϵ_{eff}) of unilateral fin lines versus the slot width ($2s$) and the metallization thickness. Cross section of employed fin line as given in Fig. 2, with the metallization thickness $d=d_1+d_2$, slit depth $c=0.326$ mm.

The effective permittivity of the fin line was calculated from the measured operating frequency and wavelength using (16) [4], [5]

$$\lambda_g = \frac{\lambda_0}{\left\{\epsilon_{\text{eff}} - \left(\frac{\lambda_0}{\lambda_c}\right)^2\right\}^{1/2}} \quad (16)$$

where λ_g is the wavelength on the fin line, λ_0 is the free-space wavelength, and λ_c is the cutoff wavelength for an equivalent air-filled ridge-loaded waveguide.

The movable short employed in the measurements was especially designed for the purpose: it consists of a metallic conducting spring contact which bridges the fins and which is moved along the fin line by a vernier mechanism. The resulting measurement accuracy for the wavelength is ± 0.5 percent.

In Fig. 3, the measured ($d=10$ and 70 μm) and calculated effective dielectric constant ϵ_{eff} is plotted versus the slot width $2s$, with the thickness of the metallization d as parameter. The value $d=10$ μm corresponds to lines using, e.g., gold-plated fins, $d=70$ μm corresponds to lines using, e.g., commercially available copper-clad substrate materials like RT/Duroid, and $d=130$ μm corresponds to a fin-line structure comparable to ordinary ridge waveguide. In this figure, the effects due to the slit in the waveguide mount are included. The thickness of the dielectric substrate was $w=0.05$ mm.

The method employed allows the consideration of infinitely small as well as of technologically realistic metallization thickness. For the limiting case $d=0$ μm, a good agreement is noticed with the theoretical results of Hofmann [3]. The numerical results for the idealized model ($d=0$ μm) especially at E-band frequencies exhibit consid-

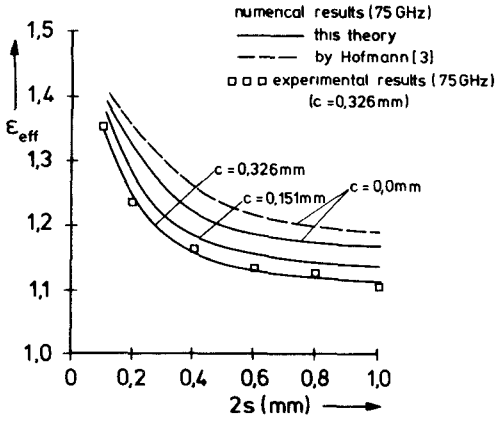

Fig. 4. Equivalent dielectric constant (ϵ_{eff}) of unilateral fin lines versus the slot width ($2s$) and the height of the longitudinal slit (c) as a parameter. Cross section of employed fin line as given in Fig. 2, with the metallization thickness $d=70$ μm.

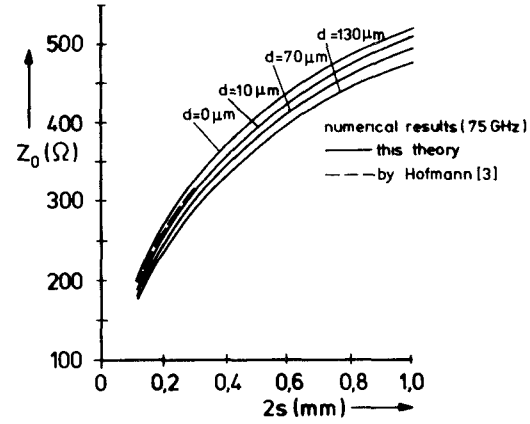

Fig. 5. Characteristic impedance (Z_0) of earthed unilateral fin line versus the slot width ($2s$) and the metallization thickness (d). Cross section of employed fin line as given in Fig. 2, with the metallization thickness $d=d_1+d_2$, slit depth $c=0.326$ mm.

erable deviations from measured effective permittivities ϵ_{eff} for practical fin lines ($d\neq 0$ μm). This shows that in the synthesis of precise millimeter-wave circuits, it is advisable to take the finite metallization thickness of realistic fin lines into consideration.

In Fig. 4, the measured and calculated effective dielectric constant ϵ_{eff} is plotted versus the slot width $2s$, with the depth c of the longitudinal slit in the waveguide mount as parameter. The zero-depth curve corresponds to the idealized model for the fin-line mount, while the realistic (experimental) case is calculated using a value of $c=0.326$ mm. In these curves, the effect due to the finite metallization thickness ($d=70$ μm) is included.

Since the present theoretical and experimental results refer to a metallization thickness $d=70$ μm, it was necessary to convert Hofmann's results ($d=0$ μm) for this model. Fig. 4 shows that especially if a large slot width $2s$ is used it is important to take the finite slit depth c into account. The agreement of the experimental and theoretical values based on this realistic calculation model is very good.

Using the described method, the electromagnetic fields of the fin line can be calculated in each subregion. From these fields, the voltage over the slit and the total longitudinal current can be computed. These values are used to define the characteristic impedance of the fin line in terms of the geometrical dimensions and the dielectric constant of the substrate material.

In Fig. 5, the fin-line characteristic impedance Z_0 is plotted versus the slot width $2s$ with the metallization thickness d as a parameter. As for the effective permittivity, the fin-line impedance shows a considerable variation with the metallization thickness d. The deviation of the characteristic impedances, e.g., for $2s=0.6$ mm, $d=0$ μm, and $d=70$ μm is about 7 percent. Fig. 5 again shows that for $d=0$ μm, the agreement between the theory presented in this paper and the theory of Hofmann [3] is very good.

The influence of the slit depth c on the fin-line impedance Z_0 is shown in Fig. 6. It is shown that especially for lines of large slot width $2s$ the variation of the characteristic impedance Z_0 from the impedance for the ideal mount $Z_0(c=0)$ can be quite considerable (about 6.5 percent for the fin line with $2s=0.6$ mm).

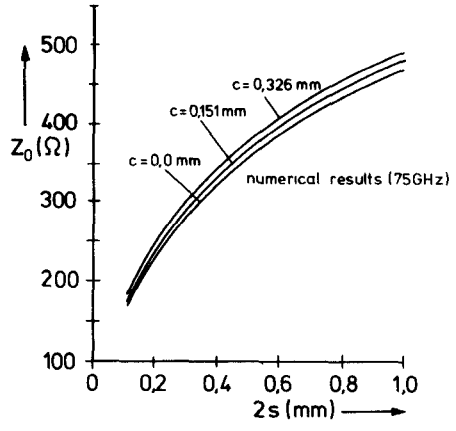

Fig. 6. Characteristic impedance (Z_0) of earthed unilateral fin line versus the slot width ($2s$) and the height of the longitudinal slit (c) as a parameter. Cross section of employed fin line as given in Fig. 2, with the metallization thickness $d=70$ μm.

IV. Conclusion

The described calculation method allows a more realistic description of the fin line than other methods published up to now. With increasing frequencies and increasing degree of integration, the significance of the technological realities, like the finite metallization thickness and the mount slit depth, increase.

The mathematical method employed has some advantages over other methods used in the literature (Transverse Resonance Method, Finite Difference Method). Since the method only needs a small number of geometrical and electrical parameters to be considered, the representation

of the boundary value problem is easy to survey. The eigenvalues calculated directly from (15) can be coordinated to the individual modes of the fin line. The method converges very rapidly and the calculated results for realistic models are in good agreement with experimental results.

REFERENCES

[1] A. Farrar and A. T. Adams, "Characteristic impedance of microstrip by the method of moments," *IEEE Trans. Microwave Theory Tech.*, vol. MTT-18, pp. 65–66, 1970.
[2] W. J. R. Hoefer and A. Ros, "Fin line parameters calculated with the TLM-method," in *1979 IEEE MTT-S Intern. Microwave Symp. Dig.* (Orlando, FL), pp. 341–343.
[3] H. Hofmann, "Dispersion of planar waveguides for millimeter-wave application," *Arch. Elektron. Übertragung.*, vol. 31, pp. 40–44, 1977
[4] P. J. Meier, "Equivalent relative permittivity and unloaded Q factor of integrated fin-line," *Electron. Lett.*, vol. 9, pp. 162–163, 1973.
[5] ——, "Integrated fin-line millimeter components," *IEEE Trans. Microwave Theory Tech.*, vol. MTT-22, pp. 1209–1216, 1974.
[6] J. P. Montgomery, "On the complete eigenvalue solution of ridged waveguide," *IEEE Trans. Microwave Theory Tech.*, vol. MTT-19, pp. 547–555, 1971.
[7] A. M. K. Saad and G. Begemann, "Electrical performance of fin lines of various configurations," *Inst. Elec Eng. J. Microwaves, Opt., Acoust (MOA)*, vol. 1, pp. 81–88, 1977.
[8] A. M. K. Saad and K. Schünemann, "A simple method for analyzing fin line structures," *IEEE Trans. Microwave Theory Tech.*, vol. MTT-26, pp. 1002–1007, 1978.

Microstrip Spiral Directional Coupler

KOJI SHIBATA, KOZO HATORI, SENIOR MEMBER, IEEE, YASUYUKI TOKUMITSU, MEMBER, IEEE, AND HIDEMITSU KOMIZO, MEMBER, IEEE

Abstract—**A new microwave directional coupler with a spiral-shaped construction is described. This coupler is named the spiral coupler and is formed by coiling two edge-coupled lines. Therefore, the size of the coupler can be greatly miniaturized. Furthermore, this coupler can achieve tight coupling much easier than the conventional coupler with edge-coupled lines on account of the multiconductor structure. The spiral couplers with a total length of a quarter-wave were fabricated on alumina ceramic substrates and resulted in 3.5-dB maximum coupling for a 40-μm strip spacing. The size of the coupler was about one-sixth of the conventional one. The spiral coupler with a total length of three quarter-waves theoretically showed 2.5-dB coupling for a 95-μm strip spacing on an alumina substrate. The achieved coupling is due to the skillful construction of the spiral. An experimental coupler fabricated on a Teflon substrate confirmed the usefulness of this approach.**

I. INTRODUCTION

AS THE SIZE of microwave integrated circuit has become much smaller in recent years, a small-sized directional coupler, especially, a wide-band 3-dB hybrid is often required. In the microwave integrated circuitry, interdigitated microstrip couplers have been developed [1], [2] since the first description by Lange [3]. But these couplers are a quarter-wave length for a single section and a much longer length for multisection couplers.

In order to obtain the small-sized directional coupler with tight coupling in wide strip spacings, a new microwave directional coupler with a spiral-shaped construction is proposed in this paper and we have named it a "spiral coupler."

The spiral coupler is formed by coiling two edge-coupled lines and is shown in Fig. 1(a), (b) as type-*A* coupler. Consequently, the size of the coupler is miniaturized. Furthermore, this coupler can achieve tight coupling much easier than the conventional coupler with edge-coupled lines, because the recoupled power which is a portion of the transmitted power increases the degree of coupling on account of the multiconductor structure.

In this paper, we describe the theoretical and experimental results and show good agreement between these results.

In the theoretical analysis, we have derived the relation between the dimensions of microstrip conductors and the circuit parameters of multiconductor transmission lines. Using these results, the performance of the coupler is calculated. In the experimental results, we show the perfor-

Manuscript received October 13, 1980; revised January 6, 1981. A condensed version of this paper has been presented at the 1980 IEEE-MTTS International Microwave Symposium, Washington, DC.

K. Shibata is with the Kitami Institute of Technology, Kitami, 090 Japan.
K. Hatori is with the Research Institute of Applied Electricity, Hokkaido University, Sapporo, 060 Japan.
Y. Tokumitsu and H. Komizo are with Fujitsu Laboratories Ltd., Kawasaki, 211 Japan.

0018-9480/81/0700-0680$00.75 ©1981 IEEE